Faraday Discussions
Cite this: *Faraday Discuss.*, 2024, **251**, 249

PAPER

Vibrational energy transfer in ammonia–helium collisions

Jérôme Loreau *[a] and Ad van der Avoird [b]

Received 22nd December 2023, Accepted 27th February 2024
DOI: 10.1039/d3fd00180f

While the rotational energy transfer of ammonia by rare gas atoms and hydrogen molecules has been the focus of many studies, little is known about its vibrational relaxation, even though transitions involving the umbrella bending mode have been observed in many astrophysical environments. Here we explore the vibrational relaxation of the umbrella mode of ammonia induced by collisions with helium atoms by means of the close-coupling method on an *ab initio* potential energy surface. We compute cross sections up to kinetic energies of 1500 cm^{-1} and rate coefficients up to a temperature of 300 K for vibrational, rotational, and inversion transitions involving the lowest two vibrational states. We show that vibrational relaxation is much less efficient than rotation–inversion relaxation, although the rate coefficients for vibrational relaxation strongly increase with the temperature. We also observe important differences for vibrationally-elastic transitions within the lowest two vibrational states, *i.e.*, for rotation–inversion transitions. These are a direct consequence of the difference in the tunnelling splitting of the lowest inversion levels.

1 Introduction

Ammonia is one of the most widely observed molecules in space. Although the observed rovibrational spectra can be used to derive physical properties of astrophysical media such as the local temperature, these spectra often display deviations from the local thermodynamic equilibrium (LTE) assumption, and their interpretation thus requires the knowledge of the rate coefficients for collisional excitation by dominant colliders in space, *i.e.*, He atoms or H_2 molecules. In this context a large number of theoretical studies have focused on computing rate coefficients corresponding to the rotation–inversion collisional excitation of ammonia by helium atoms[1–3] or H_2 molecules,[4–6] including hyperfine excitation.[7] Experimentally, ammonia can be considered a prototypical polyatomic molecule for the investigations of inelastic collisions. As such, the rotation–inversion scattering properties of (deuterated) ammonia with He or H_2 have

[a]KU Leuven, Department of Chemistry, B-3001 Leuven, Belgium. E-mail: jerome.loreau@kuleuven.be
[b]Institute for Molecules and Materials, Radboud University, Heyendaalseweg 135, 6525 AJ Nijmegen, The Netherlands

been widely explored using molecular beams with quantum state selection.[8–13] Simulations of rotational cooling of NH_3 in a helium buffer gas cell have also been carried out based on state-to-state cross sections.[14,15]

Despite this, little is known about the vibrational collisional excitation of ammonia, even though transitions involving the umbrella bending mode have been observed in many astrophysical environments, including circumstellar envelopes of various evolved stars,[16,17] protostars and star-forming regions,[18,19] and protoplanetary disks.[20] In astronomical observations, rovibrational transitions of ammonia usually involve the first excited level of the umbrella mode ν_2, at wavelengths centered around 10.5 μm, although observations of rotation–inversion transitions within the first excited vibrational state have also been reported. LTE conditions cannot be assumed for vibrational levels, and radiative transfer calculations taking into account the effect of collisions must be carried out to interpret observations.[21]

In the past few years, there has been an increased interest in the development and application of theoretical methods to treat vibrational energy transfer in inelastic collisions involving polyatomic molecules.[22] Such developments are needed in an astrochemical context, with the recent launch of the James Webb Space Telescope JWST that provides a new window to observe the universe in the infrared. Up to now, quantum scattering calculations of the vibrational excitation of polyatomic molecules have been limited to collisions with helium atoms, which have been performed for CH_3,[23] HCN,[24] C_3,[25] CO_2,[26] as well as for the torsional motion of CH_3OH,[27] and to the excitation of H_2O by H_2.[28–30] In a previous paper[31] we examined rotation–inversion transitions of NH_3 in collisions with rare gas atoms, including He, by performing quantum scattering calculations that describe the umbrella motion of ammonia explicitly. This is a form of vibrational excitation, although it occurs at an energy scale much lower than usual for vibrational modes. The computational requirements of these quantum calculations are high but they are crucial to benchmark more efficient but approximate methods.

Here we extend our previous study by exploring the vibrational excitation and relaxation of the first excited state of the umbrella mode of ammonia induced by collisions with helium atoms, by means of the close-coupling method on an *ab initio* potential energy surface. In Section 2 we briefly review the theoretical approach used in our calculations. In Section 3 we calculate cross sections for kinetic energies up to 1500 cm^{-1} and rate coefficients up to temperatures of 300 K for vibrational transitions involving the lowest two ν_2 states, as well as for rotation–inversion transitions within these vibrational states. For the latter, we show that the splitting of the lowest two inversion vibrational levels due to tunnelling leads to a dependence of the cross section upon the vibrational state. Finally, we compare our results for rotation–inversion transitions in the ground vibrational state to data from the literature. We summarize our findings in Section 4.

2 Methods

The methods have been described extensively in two previous papers,[31,32] and we only recall their main features here. The potential energy surface (PES) for the collision was calculated at the coupled-cluster level with single and double excitations and a perturbative treatment of triple excitations [CCSD(T)] with the AVQZ

basis set on all atoms in the long-range, while in the short range the explicitly-correlated variant CCSD(T)-F12 was used, with the same basis set. The four-dimensional PES $V(R, \theta, \phi, \rho)$ depends on three spherical coordinates (R, θ, ϕ) that define the position of the He atom with respect to the center of mass of NH_3, as well as on the umbrella angle ρ. 4180 *ab initio* points were computed and fitted to an expansion in spherical harmonics.

The scattering calculations are performed by means of the quantum-mechanical close-coupling (CC) method.

The Hamiltonian of the NH_3–He scattering complex, including the umbrella coordinate, can be written as

$$\hat{H} = \hat{H}_{NH_3} - \frac{\hbar^2}{2\mu R}\frac{\partial^2}{\partial R^2}R + \frac{1}{2\mu R^2}\left(\hat{J}^2 + \hat{j}^2 - 2\hat{\mathbf{j}}\cdot\hat{\mathbf{J}}\right) + V(\rho, R, \theta, \varphi) \quad (1)$$

where μ is the reduced mass of the system, $\hat{\mathbf{j}}$ is the angular momentum operator of NH_3, and $\hat{\mathbf{J}}$ is the total angular momentum operator, $\hat{\mathbf{J}} = \hat{\mathbf{j}} + \hat{\mathbf{L}}$ where $\hat{\mathbf{L}}$ is the relative angular momentum.

$\hat{H}_{NH_3}$ is the Hamiltonian describing ammonia, given by the sum of three terms:

$$\hat{H}_{NH_3} = \sum_i \frac{\hat{j}_i^2}{2I_{ii}(\rho)} + \hat{T}(\rho) + V_{umb}(\rho) \quad (2)$$

where $I_{ii}(\rho)$ are the principal moments of inertia of NH_3, which depend on the umbrella coordinate, $\hat{T}(\rho)$ is the kinetic operator corresponding to the inversion motion, and $V_{umb}(\rho)$ is a double well potential with two equivalent equilibrium angles $\rho = 112.1°$ and $\rho = 67.9°$. The double well leads to a splitting of the first two vibrational states, $\nu_2 = 0$ and $\nu_2 = 1$, into doublets with a splitting of 0.79 cm^{-1} in the ground state and 35.2 cm^{-1} in the excited state. The potential $V_{umb}(\rho)$ is parametrized analytically and fitted to reproduce the energy of these lowest four states, as well as the average $\nu_2 = 0 \rightarrow 1$ transition energy of 949.9 cm^{-1}. The expressions for these operators can be found in ref. 31 and 32.

In the CC method, the total wave function is expanded as a sum of products of radial, angular, and vibrational functions. The first four vibrational wavefunctions $\phi_\nu^\pm(\rho)$, corresponding to the symmetric (+) and antisymmetric (−) umbrella tunnelling components of the vibrational states $\nu_2 = 0$ ($\phi_0^+(\rho)$ and $\phi_0^-(\rho)$) and $\nu_2 = 1$ ($\phi_1^+(\rho)$ and $\phi_1^-(\rho)$), were obtained by solving the one-dimensional Schrödinger equation for the umbrella motion. Such an approach was previously used to interpret high resolution IR spectroscopic experiments of the NH_3–rare gas complexes in the ν_2 region.[33]

The inelastic scattering cross sections are then calculated by solving the coupled equations with the Hamiltonian (1) in the basis of rovibrational states. The scattering rate coefficients are obtained by averaging the cross sections over a Maxwell–Boltzmann distribution of velocities,

$$k_{if}(T) = \left(\frac{8}{\pi\mu\beta}\right)^{\frac{1}{2}}\beta^2\int_0^\infty E_c\sigma_{if}(E_c)e^{-\beta E_c}dE_c \quad (3)$$

where $\beta = \dfrac{1}{k_B T}$ and k_B, T and μ denote the Boltzmann constant, the kinetic temperature and the NH_3–He reduced mass, respectively.

The rotational energy levels of NH_3 are denoted as $jk\pm$, where k is the projection of the angular momentum j on the symmetry axis of the molecule. Due

to nuclear spin statistics, NH_3 occurs as *ortho*-NH_3 (for $k = 3n$, where n is an integer) and *para*-NH_3 (for $k = 3n \pm 1$) that cannot be interconverted through inelastic collisions, and for $k = 0$ half of the levels are forbidden. The lowest levels (up to $j = 4$ and $k = 3$) are shown in Fig. 1 for $\nu_2 = 0$ and for $\nu_2 = 1$. The variation in rotational structures is a consequence of the large difference in the splitting in $\nu_2 = 0$ and $\nu_2 = 1$ and can be expected to impact the dynamics of NH_3–He collisions.

The coupled equations were solved by means of the renormalized Numerov propagator for all initial states of NH_3 up to $j = 4$ and for kinetic energies in the range 0.01–1500 cm^{-1}. For energies below 50 cm^{-1}, the radial grid consists of 444 points between 4 a_0 to 80 a_0, while for energies above 50 cm^{-1} the grid extends from 4 a_0 to 40 a_0 with 211 points. The maximum value of the total angular momentum J needed to obtain convergence of the inelastic cross sections depends on the collision energy and is $J_{max} = 70$ at the highest energy considered. The size of the rotational basis set was truncated at $j_{max} = 14$.

3 Results

3.1 Rotation–inversion transitions

Cross sections and rate coefficients for rotation–inversion transitions in the ground vibrational state are available in the literature. The reference rate coefficients for astrophysical applications have been computed by Machin and Roueff[2] and cover temperatures up to 300 K. These data were obtained from quantum scattering calculations on a PES constructed by Hodges and Wheatley by fitting to scaled perturbation theory calculations.[34] This PES is qualitatively similar to the one used in the present work, although the two PESs lead to large differences in the resonance structure of the cross sections, as discussed in ref. 32 for the 11− → 11+ transition. Another difference concerns the way the inversion is taken into account. In the work of Machin and Roueff,[2] the ground tunnelling states are approximated as symmetric or antisymmetric linear combinations of delta functions localized at the equilibrium angles, which allows a calculation of rotation–inversion cross sections without the need for a potential dependent on the umbrella angle. The same approach has been used for all quantum scattering

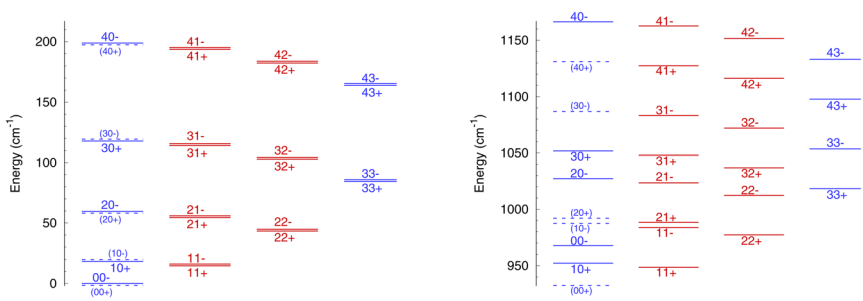

Fig. 1 Diagram of the lowest rotational energy levels of NH_3 in $\nu_2 = 0$ (left) and $\nu_2 = 1$ (right), labeled as $jk\pm$. *Ortho* levels are in blue while *para* levels are in red. Forbidden levels are indicated by the dashed lines and parentheses. The splitting in $\nu_2 = 0$ has been exaggerated for clarity's sake.

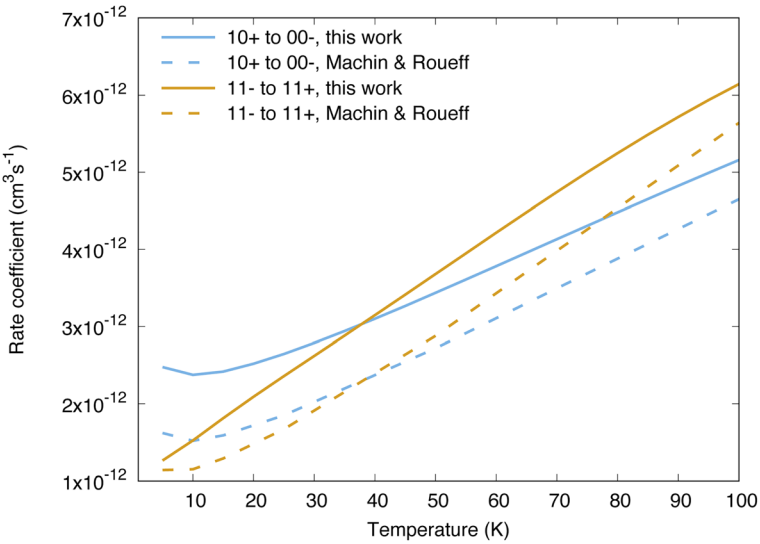

Fig. 2 Comparison between the reference rate coefficients of ref. 2 and those calculated in the present work, for the transitions 10+ → 00− and 11− → 11+.

calculations performed so far on NH_3–H_2 as well.[5,6,12] The impact of using a Hamiltonian for ammonia that depends explicitly on the umbrella coordinate on rotation–inversion transitions was discussed in ref. 31 and 32 for the 11− → 11+ transition of experimental interest, and found to be small except at low energies.

Our calculations for other transitions involving levels of NH_3 up to $j = 4$ confirm these observations. In Fig. 2 we compare the behaviour of the collisional relaxation rate coefficient for two transitions, $jk\pm = 10+ \rightarrow 00-$ in *ortho*-NH_3 and 11− → 11+ in *para*-NH_3. At low temperature the differences can be as large as 50% but decrease with increasing temperatures, indicating that the largest discrepancies originate from the low energy regime. These differences can be attributed to the quality of the underlying PESs on which the scattering calculations are performed. We further tested the impact of the explicit treatment of the umbrella motion for other rotation–inversion transitions in the ground vibrational state and found a small impact overall. Treating the first excited vibrational state requires at least four tunnelling functions. Including two more umbrella functions, for a total of six, leads to small differences on the cross sections (on the order of 5%).

It is also instructive to compare the rotation–inversion cross sections and rate coefficients in $v_2 = 1$ to those in $v_2 = 0$. It is often assumed, both by experimentalists as well as in non-LTE astrochemical models, that the scattering cross section or rate coefficient for a given rotational transition is the same within any vibrational level of a molecule excited by an atom or a molecule, which implies that the vibrational and rotational motions are decoupled. This assumption has been verified through computations, *e.g.*, for H_2O–H_2 inelastic collisions.[28] In the case of NH_3, the situation is more complex because of the splitting of the inversion levels and the fact that the splitting is dramatically different in the ground state (0.79 cm^{-1}) and in the excited state (35.2 cm^{-1}), as illustrated in Fig. 1.

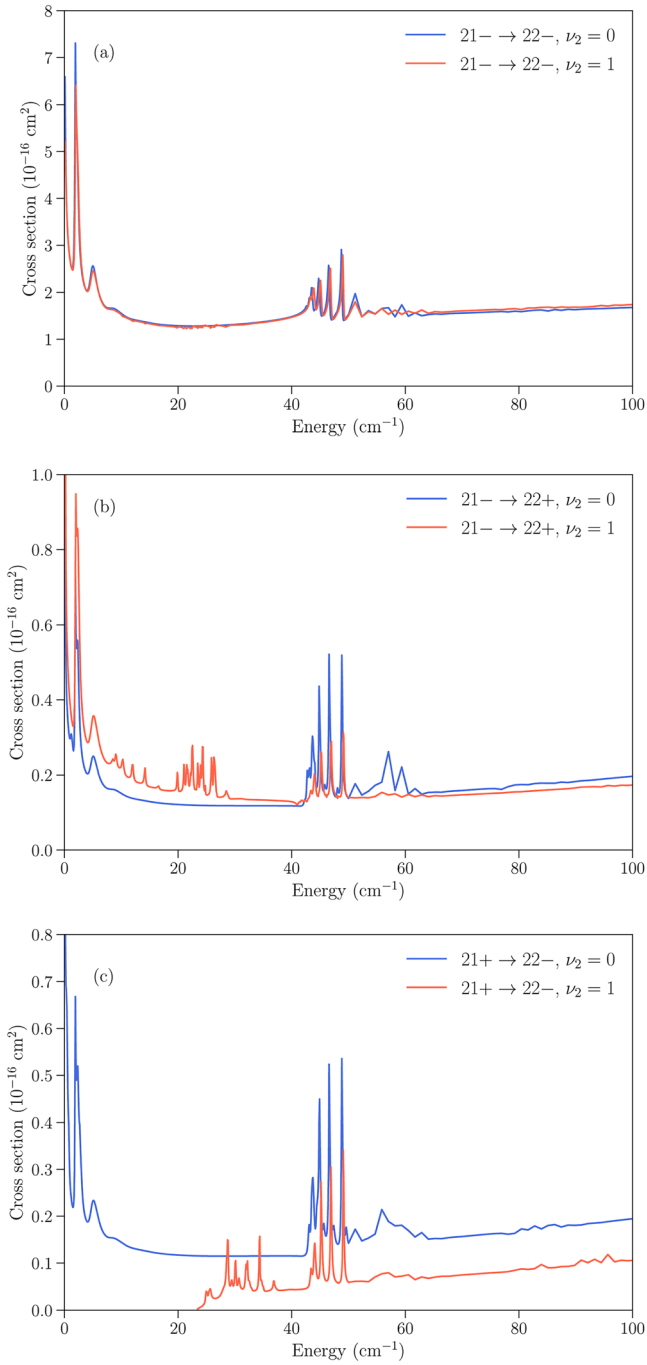

Fig. 3 Cross sections as function of kinetic energy for the rotation–inversion transitions $jk\pm = 21- \rightarrow 22-$ (panel (a)), $jk\pm = 21- \rightarrow 22+$ (panel (b)), and $jk\pm = 21+ \rightarrow 22-$ (panel (c)) in $\nu_2 = 0$ and $\nu_2 = 1$.

Several cases can then arise. The simplest is when an inelastic collision conserves the inversion symmetry (transitions $jk+ \rightarrow j'k'+$ or $jk- \rightarrow j'k'-$). Since the inversion splitting is almost independent of the quantum numbers j and k, the energy gap between the initial and final rotation–inversion state is identical in $\nu_2 = 0$ and $\nu_2 = 1$ and these transitions have cross sections that are similar. This is illustrated in panel (a) of Fig. 3 for the transition $21- \rightarrow 22-$.

The second case concerns relaxation in transitions $jk- \rightarrow j'k'+$, *i.e.* from an initial antisymmetric inversion level to a final symmetric level. Given that the splitting in $\nu_2 = 1$ is much larger than in $\nu_2 = 0$, a relaxation transition from the upper $(-)$ inversion component of an initial rotational state to the lower $(+)$ inversion component of a final rotational state corresponds to a larger energy gap in $\nu_2 = 1$ compared to $\nu_2 = 0$. As a consequence, the cross sections for those transitions are usually larger in $\nu_2 = 0$ than in $\nu_2 = 1$. This is illustrated in panel (b) of Fig. 3 for the transition $21- \rightarrow 22+$. We note that for an excitation with an initial antisymmetric inversion level ($jk- \rightarrow j'k'+$), the converse is usually true as the energy gap is smaller in $\nu_2 = 1$ compared to $\nu_2 = 0$.

The third case is for relaxation in transitions $jk+ \rightarrow j'k'-$ where the situation is reversed, with a larger energy gap in $\nu_2 = 0$ than in $\nu_2 = 1$, and an associated cross section that is usually larger for rotation–inversion transitions in $\nu_2 = 1$ than in $\nu_2 = 0$. For an excitation with an initial symmetric inversion level ($jk+ \rightarrow j'k'-$), the converse is true.

Finally, the dependence of the rotational structure on ν_2 leads to cases where transitions are exothermic in one vibrational state but endothermic in the other. An example is provided by the $jk\pm = 21+ \rightarrow 22-$ transition, which is a relaxation in $\nu_2 = 0$ but an excitation in $\nu_2 = 1$, with a threshold of about 23 cm^{-1}. This leads to large differences in the low energy regime, as can be seen in panel (c) of Fig. 3.

All the transitions illustrated in Fig. 3 display a resonance structure arising from quasi-bound states of the complex. The resonances at kinetic energies around 2 cm^{-1} and in the range 40–50 cm^{-1} are seen for all final states and can be associated with the initial $jk = 22$ state, while the resonance structure between those energies depends on the final state. It can also be noted that transitions that conserve the symmetry of the umbrella state ($+ \leftrightarrow +$ and $- \leftrightarrow -$) tend to have larger cross sections than transitions that change the umbrella state ($+ \leftrightarrow -$).[31,32]

The differences between the rotation–inversion rate coefficients in $\nu_2 = 0$ and $\nu_2 = 1$ can also be illustrated by considering the rate coefficients instead of the cross sections. Fig. 4 displays a comparison of the rate coefficients for all transitions (excitation and relaxation) starting from all initial levels $j = 0$–2 to all final levels in the range $j' = 0$–5 at a temperature of 20 K and 150 K. The rate coefficients for transitions that conserve the inversion symmetry are almost identical in the two vibrational states (this includes the elastic rate coefficients, with magnitudes of order 10^{-9} cm^3 s^{-1}). For the other cases discussed above the discrepancy is usually smaller than a factor of 3, but it can reach an order of magnitude at low temperature for weak transitions. The discrepancy is smaller at higher temperature since the difference in rotational structure in the two vibrational states becomes less and less important as the kinetic energy increases.

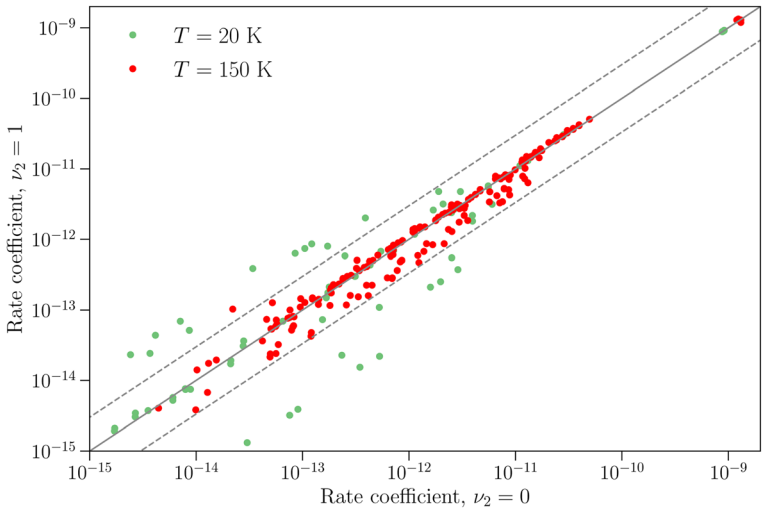

Fig. 4 Comparison of rotation–inversion rate coefficients in $\nu_2 = 0$ and $\nu_2 = 1$ at two temperatures for all transitions from all initial levels $j = 0$–2 to all final levels $j' = 0$–5. The full line correspond to equal rate coefficients, while the dashed lines denote a difference of a factor of 3.

3.2 Vibrational relaxation cross sections

We now turn to vibrationally-inelastic transitions, *i.e.* transitions $\nu_2 = 1 \rightarrow 0$. An important question concerns the magnitude of the corresponding cross sections (or rate coefficients), compared to vibrationally-elastic transitions. Vibrational relaxation cross sections are expected to be much smaller than rotational

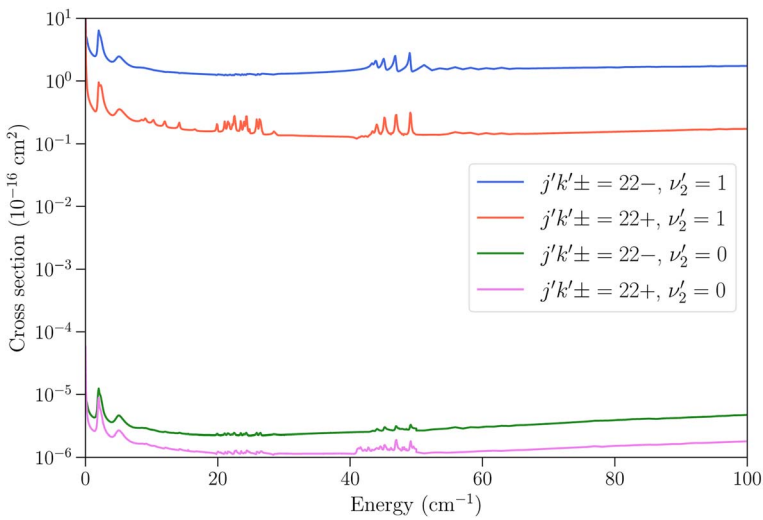

Fig. 5 Cross sections as function of kinetic energy for the transitions with initial state $jk\pm = 21-$ in $\nu_2 = 1$ and final states 22− and 22+ with $\nu'_2 = 1$ (vibrationally-elastic) and $\nu'_2 = 0$ (vibrationally-inelastic).

relaxation cross sections, given the large difference between the vibrational transition energy (~950 cm^{-1}) and the depth of the NH_3–He PES (~35 cm^{-1}), but the extent remains to be quantified.

In Fig. 5 we show the cross sections for the 21− → 22− and 21− → 22+ transitions for these two cases. The vibrational relaxation cross sections are seen to be on the order of 10^5 times smaller than the vibrationally-elastic transitions, making vibrational energy transfer seemingly very inefficient for NH_3–He collisions. The same propensity to conserve the symmetry of the umbrella state is observed as for vibrationally-elastic cross sections. The resonance structures discussed above are also seen for the vibrational relaxation cross sections, although the magnitude of the resonances is smaller.

In Fig. 6 we examine the vibrational relaxation cross sections in more detail for the initial state 11− in $\nu_2 = 1$ and all final states $j = 1$–3 in $\nu_2 = 0$ for *para*-NH_3. For all final states we observe again a larger cross section for transitions that conserve the inversion symmetry. The cross sections increase strongly with kinetic energy, as was also observed for CH_3–He collisions,[23] although for NH_3–He collisions the growth observed here is not linear.

Fig. 7 presents the distribution of the vibrational relaxation rate coefficients for all initial states with $j \leq 3$ in $\nu_2 = 1$ and all final states $j' \leq 10$ in $\nu_2 = 0$. At low temperature (20 K), the vibrational relaxation rate coefficients are on the order of 10^{-18} to 10^{-16} cm^3 s^{-1}, while the rotation–inversion rate coefficients are typically on the order of 10^{-12} to 10^{-11} cm^3 s^{-1}. However, the rate coefficients increase quickly with increasing temperature as a result of the growth of the cross sections discussed above. At 300 K the vibrational relaxation rate coefficients are on the order of 10^{-16} to 10^{-14} cm^3 s^{-1}, corresponding to an increase of two orders of magnitude compared to the values at a temperature of 20 K. It would be interesting to investigate the behaviour of the rate coefficients at higher temperatures, especially for astrochemical applications. Given the magnitude of

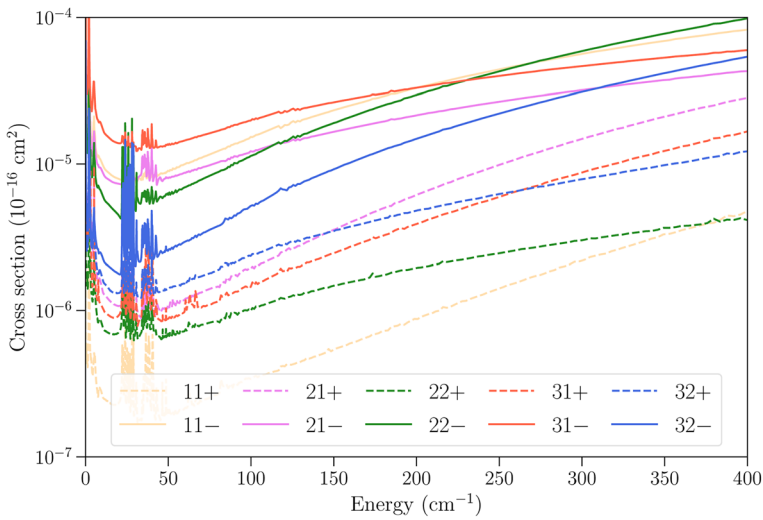

Fig. 6 Cross sections as function of kinetic energy for the vibrational relaxation transitions with initial state $jk\pm = 11-$ in $\nu_2 = 1$ and various final states in $\nu'_2 = 0$.

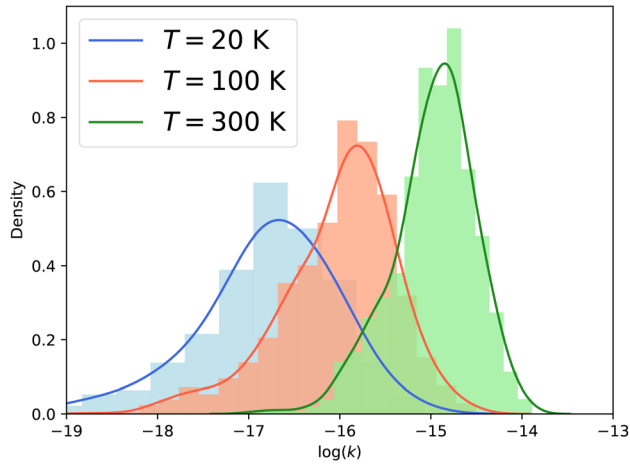

Fig. 7 Distribution of the logarithm base 10 of the vibrational relaxation rate coefficients $\nu_2 = 1 \rightarrow 0$ at three temperatures for all initial states $j = 0$–3 of *ortho*- and *para*-NH_3 and all final states $j' = 0$–10 (964 transitions). The lines represent kernel density estimates.

the rate coefficients, and the large number of rotational states in the ground vibrational level that are open, vibrational relaxation could be efficient in warm astrophysical environments, although the state-to-state rate coefficients are several orders of magnitude smaller than the vibrationally-elastic ones. This will require the use of different scattering methodology, such as that presented in ref. 26, since the fully quantum-mechanical CC calculations performed here become intractable at the higher energies required to obtain converged rate coefficients above 300 K.

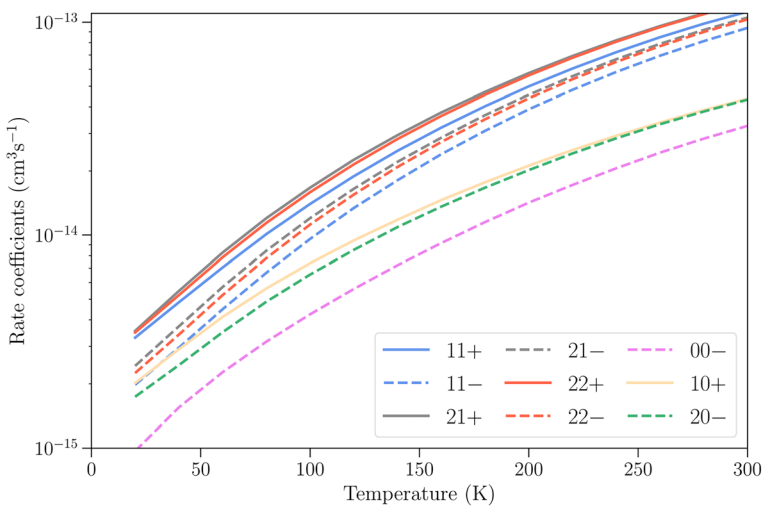

Fig. 8 Total vibrational relaxation rate coefficients $\nu_2 = 1 \rightarrow 0$ for various initial rotation–inversion states of *para*-NH_3 and *ortho*-NH_3, summed over all final states. Symmetric and antisymmetric initial inversion states are denoted by full and dashed lines, respectively.

Finally, we present in Fig. 8 the total vibrational relaxation rate coefficients for all initial rotation–inversion states with $j = 0$–2 summed over all final states. The total rate coefficients vary from 10^{-15} cm^3 s^{-1} at $T = 20$ K and increase up to 10^{-13} cm^3 s^{-1} at $T = 300$ K for initial rotation–inversion states in *para*-NH_3, corresponding to the increase with temperature discussed earlier at the state-to-state level. For a given initial rotational level, the total vibrational relaxation rate coefficients are slightly larger for symmetric inversion levels than for antisymmetric ones. The rate coefficients for levels 21+ and 22+ or 21− and 22− are virtually identical, but larger than those for 11+ and 11− respectively. Moreover, they are larger for *para*-NH_3 than for *ortho*-NH_3 by a factor of about 2. This difference originates from the difference in the number of final rotation–inversion states available in $\nu_2 = 0$ for vibrational relaxation, which is roughly twice as large for *para*-NH_3 than for *ortho*-NH_3.

4 Conclusions and outlook

In the present paper we have presented a study of vibration–rotation–inversion transitions in NH_3 induced by collisions with He atoms by considering the umbrella inversion vibrational mode of ammonia. We obtained cross sections for collision energies up to 1500 cm^{-1}, and rate coefficients for temperatures up to 300 K. The calculations relied on an accurate four-dimensional PES used in quantum-mechanical scattering calculations. Important differences were found with reference data for the inelastic rate coefficients in the ground vibrational state, which were attributed to the use of a more recent PES. There are also large differences between pure rotation–inversion cross sections within the ground vibrational state or the first vibrational excited state. These follow from the difference in the inversion splitting in the ground and excited umbrella vibrational levels. For transitions that conserve the inversion symmetry, rotation–inversion cross sections are virtually identical in the two vibrational levels.

The vibrational relaxation cross sections are about five orders of magnitude smaller than the vibrationally-elastic cross sections at low energy, and the same observation is made for the rate coefficients at low temperature (below 50 K). However, vibrational relaxation cross sections display a strong increase as function of collision energy. The rate coefficients for vibrationally-inelastic transitions are therefore much larger at high temperature, with a typical increase of more than two orders of magnitude between 20 K and 300 K, while the vibrationally-elastic rate coefficients increase much less rapidly. It thus appears that vibrational relaxation of NH_3 by He atoms can be quite efficient at high temperature, given the large number of rotation–inversion states that are populated through inelastic collisions.

The results presented here are however limited in several respects. First, we only considered initial rotational levels of NH_3 with $j < 5$. In order to use these rate coefficients in a non-LTE radiative transfer model, many more initial states would need to be considered. Secondly, the temperature was limited to 300 K, which is unlikely to be high enough for applications to warm astrophysical environments. This limitation is due to a combination of factors. First, the PES used here needs to be completed by adding points in the short range to be used for high energy collisions (above 3000 cm^{-1} of total energy). Second, at high energy there are too many open rotational levels, so that the rotational basis used in the close-

coupling expansion becomes too large for the current available computational resources. A promising approach to generate data sets of rate coefficients for astrophysical applications would be to employ approximate methods such as those presented in ref. 26, which allow a drastic reduction of the computational requirements. On the other hand, highly accurate quantum-mechanical calculations such as presented here are still purposeful to benchmark approximate methods. Vibrational relaxation from the second excited state of the umbrella mode could also be treated by the same methods. Since the second excited state is above the inversion barrier, the state-to-state rate coefficients can be expected to be completely different from those in the first two vibrational states.

Finally, the vibrational relaxation by collisions with H_2 molecules should also be investigated. It is expected to be more favorable than for He since relaxation can then also occur to excited rotational states of H_2, which has been shown to be much more efficient than for H_2 ($j = 0$) in the case of H_2O.[29,30]

Conflicts of interest

There are no conflicts to declare.

Acknowledgements

We thank Milena Rohrs and Gerrit Groenenboom for useful discussions. J. L. acknowledges support from KU Leuven through grant no. C14/22/082. The calculations presented in this work were performed on the VSC clusters (Flemish Supercomputer Center), funded by the Research Foundation Flanders (FWO) and the Flemish Government.

Notes and references

1 S. Green, *J. Chem. Phys.*, 1976, **64**, 3463.
2 L. Machin and E. Roueff, *J. Phys. B: At., Mol. Opt. Phys.*, 2005, **38**, 1519.
3 B. Yang and P. C. Stancil, *Eur. Phys. J. D*, 2008, **47**, 351.
4 G. Danby, D. R. Flower, P. Valiron, E. Kochanski, L. Kurdi and G. H. F. Diercksen, *J. Phys. B: At. Mol. Phys.*, 1987, **20**, 1039.
5 S. Maret, A. Faure, E. Scifoni and L. Wiesenfeld, *Mon. Not. R. Astron. Soc.*, 2009, **399**, 425.
6 S. Demes, F. Lique, J. Loreau and A. Faure, *Mon. Not. R. Astron. Soc.*, 2023, **524**, 2368–2378.
7 J. Loreau, A. Faure, F. Lique, S. Demes and P. J. Dagdigian, *Mon. Not. R. Astron. Soc.*, 2023, **526**, 3213.
8 J. Schleipen and J. ter Meulen, *Chem. Phys.*, 1991, **156**, 479.
9 F. Pirani, L. Roncaratti, L. Belpassi, F. Tarantelli and D. Cappelletti, *J. Chem. Phys.*, 2011, **135**, 194301.
10 O. Tkac, A. K. Saha, J. Onvlee, C.-H. Yang, G. Sarma, C. K. Bishwakarma, S. Y. T. van de Meerakker, A. van der Avoird, D. H. Parker and A. J. Orr-Ewing, *Phys. Chem. Chem. Phys.*, 2014, **16**, 477–488.
11 O. Tkac, A. K. Saha, J. Loreau, Q. Ma, P. J. Dagdigian, D. H. Parker, A. van der Avoird and A. J. Orr-Ewing, *Mol. Phys.*, 2015, **113**, 3925.

12 Q. Ma, A. van der Avoird, J. Loreau, M. Alexander, S. Y. T. van de Meerakker and P. J. Dagdigian, *J. Chem. Phys.*, 2015, **143**, 044312.
13 Z. Gao, J. Loreau, A. van der Avoird and S. Y. T. van de Meerakker, *Phys. Chem. Chem. Phys.*, 2019, **21**, 14033.
14 O. Schullian, J. Loreau, N. Vaeck, A. van der Avoird, B. R. Heazlewood, C. J. Rennick and T. P. Softley, *Mol. Phys.*, 2015, **113**, 3972.
15 M. J. Doppelbauer, O. Schullian, J. Loreau, N. Vaeck, A. van der Avoird, C. J. Rennick, T. P. Softley and B. R. Heazlewood, *J. Chem. Phys.*, 2017, **146**, 044302.
16 J. D. Monnier, W. C. Danchi, D. S. Hale, P. G. Tuthill and C. H. Townes, *Astrophys. J.*, 2000, **543**, 868–879.
17 K. T. Wong, K. M. Menten, T. Kamiński, F. Wyrowski, J. H. Lacy and T. K. Greathouse, *Astron. Astrophys.*, 2018, **612**, A48.
18 C. Knez, J. H. Lacy, N. J. Evans, E. F. van Dishoeck and M. J. Richter, *Astrophys. J.*, 2009, **696**, 471.
19 J. C. Barentine and J. H. Lacy, *Astrophys. J.*, 2012, **757**, 111.
20 J. R. Najita, J. S. Carr, S. D. Brittain, J. H. Lacy, M. J. Richter and G. W. Doppmann, *Astrophys. J.*, 2021, **908**, 171.
21 J. H. Lacy, *Astrophys. J.*, 2013, **765**, 130.
22 T. Selim, A. van der Avoird and G. C. Groenenboom, *J. Chem. Phys.*, 2022, **157**, 064105.
23 Q. Ma, P. J. Dagdigian and M. H. Alexander, *J. Chem. Phys.*, 2013, **138**, 104317.
24 T. Stoecklin, O. Denis-Alpizar, P. Halvick and M.-L. Dubernet, *J. Chem. Phys.*, 2013, **139**, 124317.
25 T. Stoecklin, O. Denis-Alpizar and P. Halvick, *Mon. Not. R. Astron. Soc.*, 2015, **449**, 3420–3425.
26 T. Selim, A. van der Avoird and G. C. Groenenboom, *J. Chem. Phys.*, 2023, **159**, 164310.
27 D. Rabli and D. R. Flower, *Mon. Not. R. Astron. Soc.*, 2011, **411**, 2093–2098.
28 T. Stoecklin, O. Denis-Alpizar, A. Clergerie, P. Halvick, A. Faure and Y. Scribano, *J. Phys. Chem. A*, 2019, **123**, 5704–5712.
29 L. Wiesenfeld, *J. Chem. Phys.*, 2021, **155**, 071104.
30 R.-M. Garcia-Vazquez, A. Faure and T. Stoecklin, *ChemPhysChem*, 2024, **25**, e202300698.
31 J. Loreau and A. van der Avoird, *J. Chem. Phys.*, 2015, **143**, 184303.
32 K. B. Gubbels, S. Y. T. van de Meerakker, G. C. Groenenboom, G. Meijer and A. van der Avoird, *J. Chem. Phys.*, 2012, **136**, 074301.
33 Y. Belkhodja, J. Loreau, A. van der Avoird, Y. Berger and P. Asselin, *Phys. Chem. Chem. Phys.*, 2021, **23**, 10864.
34 M. P. Hodges and R. J. Wheatley, *J. Chem. Phys.*, 2001, **114**, 8836.